Computers & Geosciences 148 (2021) 104687

Contents lists available at ScienceDirect

Computers and Geosciences

journal homepage: www.elsevier.com/locate/cageo

Constructing large-scale complex aquifer systems with big well log data: Louisiana model

Hamid Vahdat-Aboueshagh [1], Frank T.-C. Tsai, Ph.D. [2,*]

Department of Civil and Environmental Engineering, Louisiana State University, 3255 Patrick F. Taylor Hall, Baton Rouge, LA, 70803-6405, USA

ARTICLE INFO

Keywords:
Lithofacies
Aquifer systems
Modeling
Well logs
Big data
Louisiana

ABSTRACT

This study introduces a lithofacies modeling method to construct a complex Louisiana stratigraphy model up to depth of 900 m using more than 114,000 well logs. Lithofacies intervals in one well log can be as many as 76. Louisiana comprises a number of interconnected aquifer systems and distinct geological features, such as angular unconformities, domes, and faults. The method contains processes of tessellation, discretization, translation, and interpolation to accommodate these geological features. First, the model domain is tessellated into tiles. Formations have the same dip direction within the same tile, but may have varying dip angles. Each tile is then discretized into computational cells. The data of well logs in and around a tile are translated to a non-dipping domain. A tile-lithofacies model for each tile is then constructed by interpolating well log data in the non-dipping domain. Tile-lithofacies models for all tiles are generated concurrently through parallel computing. Finally, the tile-lithofacies models are back-translated to the dipping domain and are assembled to form a complex lithofacies model. The method was applied to construct a Louisiana stratigraphy model as deep as 800 m. The model revealed two different depositional patterns in southeastern Louisiana likely due to depositional dissimilarity of the ancestral Mississippi River and Tennessee River. The major recharge zones appear to be in northwestern, southeastern, and west-central Louisiana. These recharge zones represent essential outcrop zones for Louisiana's principal aquifers. The model confirmed hydraulic connections of the Mississippi River and the Red River to their underlying alluvial sands. Hydraulic connections among different aquifer systems were also revealed. The Louisiana lithofacies model offers valuable information to improve current knowledge about Louisiana's geology and demonstrates a method potential for large-scale lithofacies modeling.

1. Introduction

Modeling geological stratigraphy over large-scale domains becomes achievable owing to large data storage and high computing power, especially for applications in the field of hydrogeology (D'Agnese et al., 1999; Döll et al., 2014) with either simplified or conceptual models (de Graaf et al., 2015; Goderniaux et al., 2009; Maxwell et al., 2015; Sutanudjaja et al., 2011). There has been an increasing uptake of 3D mapping and modeling methods at geological survey organizations (GSOs). MacCormack et al. (2019) highlights the recent successes, accomplishments, and challenges experienced by GSOs in the development and deployment of their 3D modeling programs. Stratigraphy models play an important role in understanding geological formations for groundwater studies, sustainable resource development, environmental protection, and public safety.

Various methods were developed to model stratigraphy. Conceptual methods such as sequence stratigraphy (Haq, 1991; Posamentier and James, 1993; Posamentier and Allen, 1993; Yoshida et al., 2007; Catuneanu et al., 2011; Catuneanu, 2019) identify chronostratigraphic surfaces based on spatial patterns of depositions within the geological timeline of sedimentary processes. Geostatistics-based methods provide detailed facies variation, including occurrence probability (Dowd, 1991; Chilès and Delfiner, 2009; Wackernagel, 2013). Among various geostatistical approaches are multi-point simulation (Strebelle, 2002; Liu

* Corresponding author.
E-mail addresses: hvahda1@lsu.edu (H. Vahdat-Aboueshagh), ftsai@lsu.edu (F.T.-C. Tsai).

[1] Hamid Vahdat-Aboueshagh, Ph.D. student, has substantial contributions to Conceptualization; Methodology; Formal analysis; Investigation; Validation; Visualization; Roles/Writing - original draft; and Writing - review & editing.

[2] Frank Tsai, student's advisor, has substantial contributions to Conceptualization; Methodology; Investigation; Funding acquisition; Project administration; Supervision; Roles/Writing - original draft; and Writing - review & editing.

https://doi.org/10.1016/j.cageo.2021.104687
Received 16 February 2020; Received in revised form 2 January 2021; Accepted 5 January 2021
Available online 12 January 2021
0098-3004/

et al., 2004; Hu and Chugunova, 2008), transition probability simulation (Journel and Alabert, 1989; Weissmann et al., 1999; Lee et al., 2007; He et al., 2014), and two-point variogram methods (Johnson and Dreiss, 1989; Johnson, 1995). The geostatistical methods are robust at integrating different sources of information; however, they are very sensitive to input datasets and can be computationally exhaustive for large-scale modeling with abundant data. The conceptual models in large scales can be combined with geostatistic methods in finer scales to create a detailed stratigraphy for a large domain. Another class of stratigraphy modeling methods is the horizon method (Lemon and Jones, 2003; Wu et al., 2005; Caumon et al., 2009; Gallerini and De Donatis, 2009; Touch et al., 2014) which interpolates upper and lower limits of stratigraphic units using lithologic bed data at borehole locations and cross sections. The simplicity and computational efficiency in dealing with abundant data make the horizon method a suitable approach for large-scale facies modeling.

In developing stratigraphy models, collecting data and processing data are very challenging (Chang and Park, 2004). A big volume of data introduces a computational burden as well as complexity (Katal et al., 2013; Sivarajah et al., 2017). Lithological data may be integrated from different sources such as lithologic logs and electric logs. Cognitive geological knowledge may be also used to inform the model (Royse, 2010). Various types of well log information, distribution and density of well logs in a study domain, and frequent variation of lithofacies in boreholes add to the complexity of lithofacies modeling (Wycisk et al., 2009; Chesnaux et al., 2011; Zhu et al., 2012; Jørgensen et al., 2015; Song et al., 2020). Unifying different sources of well log data into the same class is the key mechanism to deal with big data complexity. In this study the term "big well log data" refers to a large volume of well log dataset.

This study introduces a lithofacies modeling method utilizing lithologic information in a big well log dataset to build a large-scale complex lithofacies model. The modeling processes include tessellation, discretization, translation, and interpolation to cope with geological complexities such as structural dips, domal uplifts, angular unconformities, and faults. The lithofacies modeling method is demonstrated through the development of a Louisiana lithofacies model. This study does not intend to find correlation among well logs. Instead, the correlation and stratigraphic units in Louisiana have been established by the USGS studies (Hosman 1996; Weiss 1990) that determine the dip directions and dip angles. These stratigraphic units are coarse. This study introduces the proposed method and employs a vast number of well logs to construct detailed sand-clay facies structures along the dip directions and dip angles. The modeling processes working together with big well log data present an appealing approach.

2. Methodology

2.1. Well logs

Well logs are the key source of data in understanding dipping geological structures. Well logs include drillers' logs, geotechnical borings, and wireline electric logs. Geotechnical borings have high-quality lithologic descriptions using the Unified Soil Classification System (ASTM, 2017), but are usually shallow (less than 10 m). Electric logs provide more accurate bed boundaries for lithofacies (Hilchie, 1982) compared to other types of well logs. However, electric logs are usually not abundant and often miss information for top 30 m–40 m due to the well casing. Drillers' logs are produced by drillers during drilling. Lithologic descriptions in drillers' logs are sometimes ambiguous or unrecognizable. Drillers' logs with unrecognizable lithological descriptions shall be discarded.

2.2. Model domain tessellation and discretization

In order to cope with changes in structural dip direction (e.g., domes) and discontinuity (e.g., faults), this study tessellates the model domain into a collection of tiles. Geological formations in each tile are assumed to have the same dip direction, but dip angle can vary in depth. Different tiles may have different dip directions. Therefore, a region of changing strikes is made of many tiles. A tile is further discretized into a number of computational cells in order to build a lithofacies model. The size of computational cells depends on the desired accuracy. For example, areas surrounding fault traces may be given finer discretization in order to capture the discontinuity at faults.

The proposed method uses lithological data, well location, dip direction, and slopes of the upper and lower inclined planes in geological formations as input data to generate lithofacies for computational cells. Consider a dipping geological structure for a tile shown in Fig. 1. The dip direction α is the same within a tile, which results in a constant strike. The slope represents the tangent value of a dip angle. This study assumes linear slope increase from slope s_1 to slope s_2. In the plan view (Fig. 1a), the tile is discretized into a number of computational cells. A pivot point (x_P, y_P) is at the southwest corner of the tile, where a pivot strike passes. The pivot strike is perpendicular to the dip direction. The pivot strike divides the tile into an updip domain and a downdip domain. A pivot plane is a vertical plane passing the pivot strike.

Given a vertical well location Q in the tile, a fold line AA′ passes Q and intersects the pivot strike at location B. The cross-sectional view of the fold line is shown in Fig. 1b. At location B, the slope at elevation z_1 is s_1 and at elevation z_2 is s_2. The inclined plane E_1 passes elevation z_1 with slope s_1 and the inclined plane E_2 passes elevation z_2 with slope s_2. Elevations above the plane E_1 have the same slope as s_1. Elevations below the plane E_2 have the same slope as s_2. The plane E_1 and the plane E_2 intercept at the line O. The inclined plane E between the plane E_1 and the plane E_2 passes elevation z_Q at the vertical well location Q and elevation $z_{Q'}$ at the location B or the pivot plane. Elevations z_1, z_2 and, $z_{Q'}$ are vertically beneath the location B. In what follows, the key parameters s_1, s_2, z_1 and z_2 are used to determine a dipping stratigraphy.

2.3. Domain transformation: from dipping domain to non-dipping domain

Using well logs to directly construct a stratigraphy of varying slopes of dips in a dipping domain can be difficult. Instead, translating all well log data into a non-dipping domain and performing lithofacies modeling in horizontal planes is much easier than directly interpolating lithofacies modeling in the dipping domain. A similar concept was suggested by Mallet (2004, 2014), which transforms horizons from a curvilinear system to a rectilinear system. Lithofacies modeling is performed in the rectilinear system. The domain transformation in this study is made simpler than Mallet (2004) by tessellating a non-linear domain (changing dip direction and slope) into a number of semi-linear domains (tiles) with constant dip direction, but varying slope in each tile. For each tile, well log data are translated from a dipping domain to a non-dipping domain, and then are interpolated to computational cells on horizontal planes. The resulting lithofacies distribution is then translated back to the dipping domain.

To translate well log data at location Q to a non-dipping domain, the vertical translation for elevation z_Q (Fig. 1b) is calculated based on the horizontal distance (d_Q) from the location Q to the pivot plane and the slope (s_Q) at elevation z_Q:

$$\Delta z_Q = d_Q s_Q \tag{1}$$

where Δz_Q is the vertical translation at elevation z_Q. The greater the distance d_Q, the larger the vertical translation. The horizontal distance d_Q is calculated by (Spiegel, 1986)

$$d_Q = (x_Q - x_P)\cos\alpha + (y_Q - y_P)\sin\alpha \tag{2}$$

where x_Q and y_Q are the coordinates of the well location Q. d_Q is negative if the well location Q is in the updip domain and is positive if the well

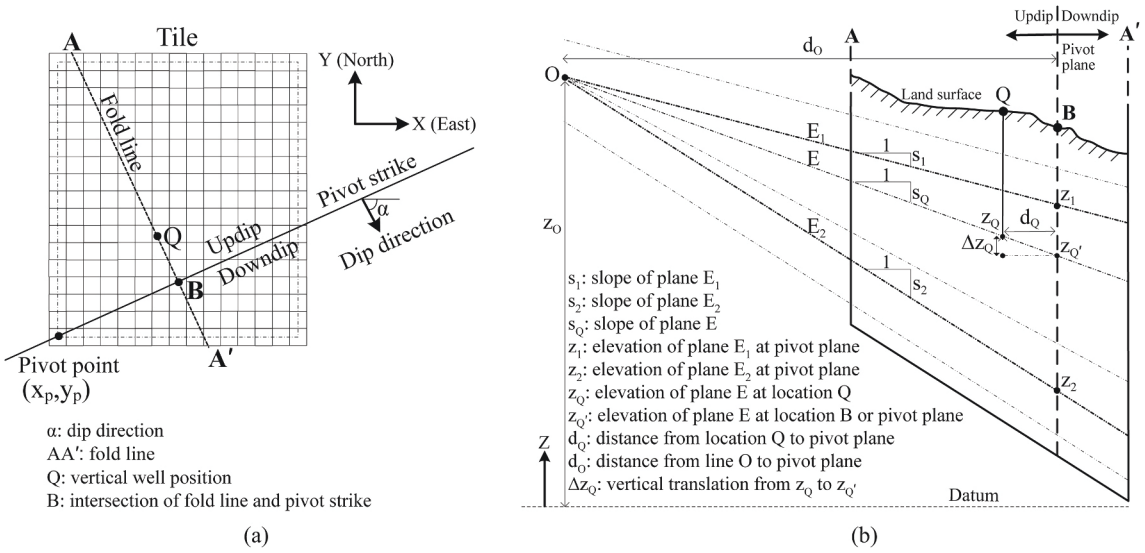

Fig. 1. (a) The plan view of a discretized tile, and (b) the cross-sectional view of the fold line AA'.

location is in the downdip domain.

Given the slope s_1 and slope s_2, where $s_2 > s_1$ in Fig. 1b, a slope at any elevation z_Q vertically beneath location Q is determined as follows

$$s_Q = \begin{cases} s_1 & \text{if } z_{Q'} > z_1 \\ \dfrac{z_O - z_Q}{d_O - d_Q} & \text{if } z_2 \le z_{Q'} \le z_1 \\ s_2 & \text{if } z_{Q'} < z_2 \end{cases} \tag{3}$$

where s_Q is the slope at elevation z_Q. $z_{Q'}$ is the translated elevation of z_Q, z_O is the elevation of the line O. Elevations above the inclined plane E_1 have the same slope s_1, which is defined at elevation z_1 in the pivot plane. Elevations below the inclined plane E_2 have the same slope s_2, which is defined at elevation z_2 in the pivot plane. Based on the trigonometry, the slope s_Q is $\frac{z_O - z_Q}{d_O - d_Q}$ for any elevation between the planes E_1 and E_2. d_O is the horizontal distance from line O to the pivot plane. d_O is calculated by

$$d_O = \frac{z_1 - z_2}{s_2 - s_1} \tag{4}$$

Therefore, $z_{Q'}$ is calculated as

$$z_{Q'} = z_Q + \Delta z_Q \tag{5}$$

If the formations have the same dip angle (i.e. $s_1 = s_2$) throughout the depth, the slope at elevation z_Q is s_1 (i.e. $s_Q = s_1$).

2.4. Lithofacies modeling on non-dipping domain

This study adopted the lithofacies modeling approach from Pham and Tsai (2017) to construct a stratigraphy on a non-dipping domain. Binary values are assigned to sand facies and clay facies. Well log data are mapped to a non-dipping domain. Sand and clay facies at well log locations are interpolated on horizontal planes at different depths via indictor natural neighbor interpolation method (Tsai, 2009)

$$\widehat{I}(\mathbf{x}_0) = \sum_{i=1}^{N} w_i I_i \tag{6}$$

where $\widehat{I}$ is the estimated indicator value at unsampled location $\mathbf{x}_0$, I_i is the indicator value at well log i, w_i is the natural neighbor weight for well log i, and N is the number of well logs. $I = 1$ refers to sand facies. $I = 0$ refers to clay facies. The weights are calculated by the natural neighbor interpolation method (Green and Sibson, 1978; Sukumar et al., 2001). Further details about the natural neighbor method can be found in Boissonnat and Cazals (2002) and Watson (1999). A Fortran program – Tile (Green and Sibson, 1978) was used to calculate the natural neighbor weights in equation (6). A cutoff value that determines $\widehat{I}$ to be either a sand or a clay facies can be approximated based on the sand facies fraction of the well log data in a tile (Elshall et al., 2013).

Similar to the indicator kriging, Tsai (2009) derived conditional estimation variance for using non-kriging weights in equation (6). It is noted that the indictor natural neighbor interpolation method is one of many interpolation methods, but is computationally efficient. A three-dimensional stratigraphy model in the non-dipping domain is resulted by stacking up all horizontal planes.

2.5. Back-translating non-dipping stratigraphy to dipping domain

After a stratigraphy is determined in a non-dipping domain, estimated lithofacies at any location Q at elevation $z_{Q'}$ is back-transformed to corresponding depth z_Q in the dipping domain by:

$$z_Q = z_{Q'} - \Delta z_Q \tag{7}$$

where Δz_Q is calculated by equation (1).

The geometry of a non-dipping domain changes after the translation from its dipping domain. Fig. 2a illustrates transformation of a dipping formation to a non-dipping formation. The lithofacies in the non-dipping domain stretch due to increasing slope with depth and lie horizontally. To cope with an angular unconformity in a tile as shown in Fig. 2b, the mildly dipping stratum (younger) is separated from the steeply dipping stratum (older). As a result, lithofacies estimation is conducted separately in two non-dipping domains. Then, the estimated lithofacies are transformed back and merged to the same tile. Fig. 2b illustrates the Louisiana geology, where the Holocene-Pleistocene alluvial deposits eroded and replaced partial Tertiary deposits. Because each tile can be modeled independently from the other tiles, the modeling can be efficiently performed by parallel computing.

One caveat in tessellating the domain is unavoidably creating interpolation discontinuity in dip direction and dip angle across tile boundaries, which may result in lithofacies discontinuity at tile boundaries. Other factor contributing to boundary discontinuity is lack of deep wells in a tile. The interpolation discontinuity can be minimized by refining the tile size and incorporating more well logs outside the tile of interest. However, the interpolation discontinuity issue arising from deep well scarcity is difficult to resolve and artifacts around tile

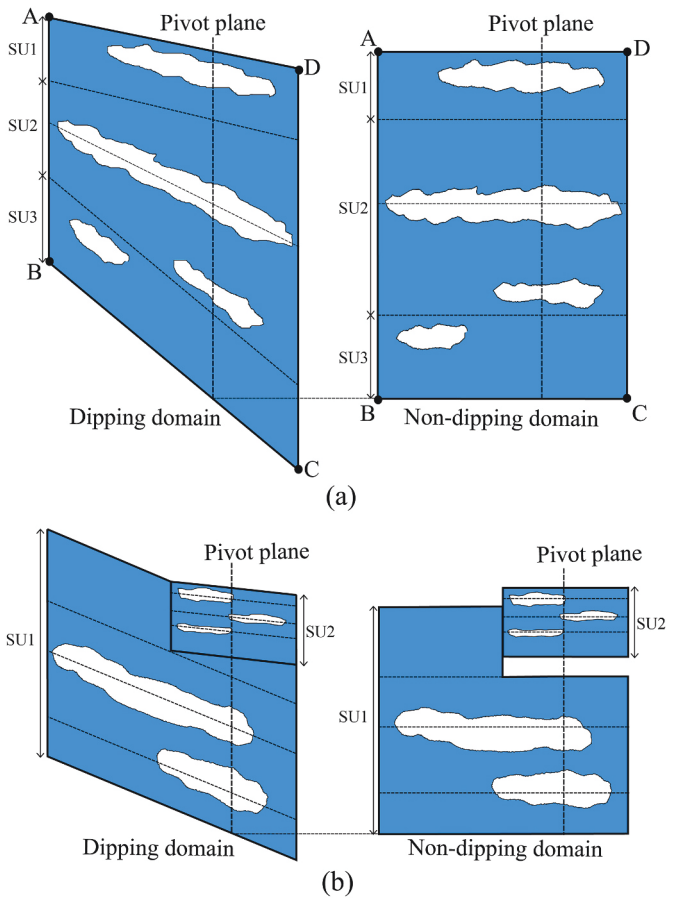

Fig. 2. Translation from dipping domains to non-dipping domains: (a) three stratigraphic units with increasing slope in depth, and (b) two stratigraphic units with angular unconformity. Blue and white colors represent two different lithofacies. SU: Stratigraphic Unit. (For interpretation of the references to color in this figure legend, the reader is referred to the Web version of this article.)

boundaries may remain. If a tile boundary is formed by a fault line, then the well logs across the fault line are not included for interpolation in order to maintain lithofacies discontinuity at the fault line.

3. Study area: state of Louisiana (USA)

The proposed methodology was employed to develop a state lithofacies model for Louisiana, USA. The state covers an area of about 135,000 km^2 (U.S. Census Bureau, 2010). Topography decreases from the upland terraces in the north to the relatively flat Chenier Plain and the Mississippi River Delta Plain in the south adjacent to the Gulf of Mexico. Fig. 3 shows the major rivers, lakes, coastal plains, fault traces and the Sabine Uplift area in Louisiana. The Eocene-Pleistocene formations are partly overlain by the Holocene sediments mainly from the alluvial depositions of the Red River, the Ouachita River, and the Mississippi River (Horton, 2017).

There are a few major geological structures in Louisiana: dips, faults, and domes. The dip angle and dip direction are not constant over the entire state. There are also angular unconformities formed by flat-lying alluvial deposits over steep-dipping formations (Hosman, 1996). In addition, there are families of faults in the southern Louisiana, of which the Baton Rouge fault system is the most distinct fault system (Heinrich, 2005; McCulloh and Heinrich, 2012). The Sabine Uplift is an important Cretaceous basement block, which extends from easternmost Texas to northwestern Louisiana (Halbouty and Halbouty, 1982).

The areal extent of 13 major freshwater aquifer systems and their vertical sequence in Louisiana are shown in Fig. 4 (Smoot, 1986). The

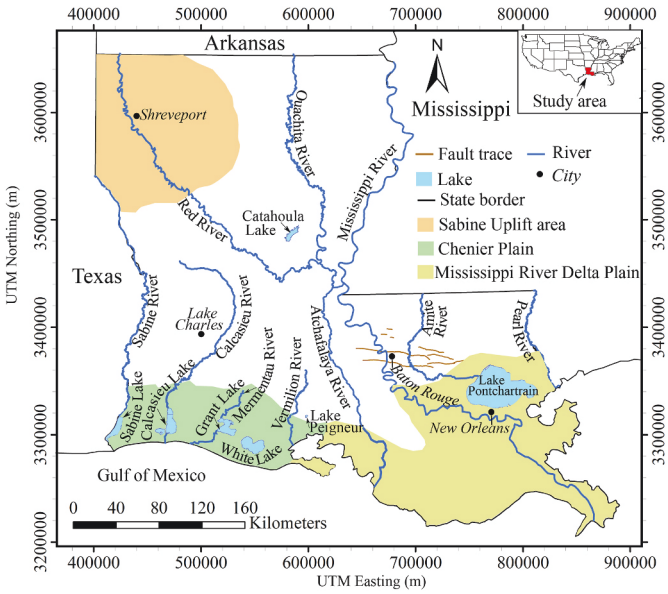

Fig. 3. Study area (Louisiana) that includes major rivers, lakes, coastal plains, fault traces in the southeast, and the Sabine Uplift in the northwest. The coordinates are in NAD83/UTM zone 15 N.

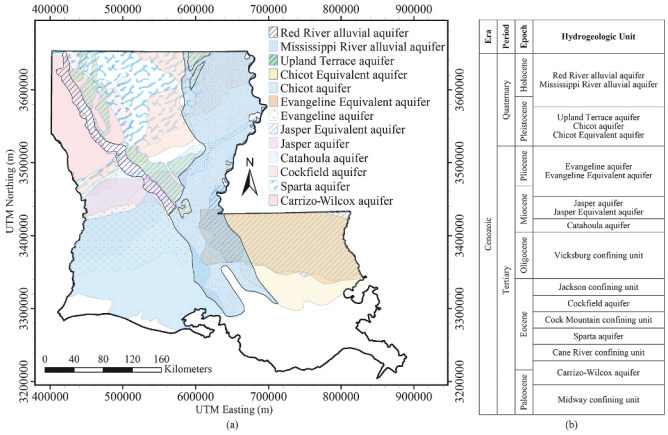

Fig. 4. (a) Areal extent of the freshwater aquifers in Louisiana, and (b) vertical sequence of the hydrogeologic units of Louisiana, modified from Smoot (1986).

Paleocene-Eocene Carrizo-Wilcox and Sparta aquifers are overlain by the Pleistocene-Holocene Red River alluvial aquifer (RRAA) and the Upland Terrace aquifer in the northwest. The Eocene Cockfield aquifer is above the Sparta aquifer and is overlain by the Mississippi River alluvial aquifer (MRAA) of Pleistocene-Holocene age. The Oligocene-Miocene Catahoula aquifer underlies the MRAA, the RRAA, and the Upland Terrace aquifer in the central Louisiana and underlies the Miocene Jasper aquifer in the western Louisiana. In the southwest, the Evangeline aquifer of Miocene-Pliocene age overlies the Jasper aquifer and is overlain by the Pleistocene Chicot aquifer system. The Jasper Equivalent aquifer, Evangeline Equivalent aquifer, and Chicot Equivalent aquifer in the southeast are from the Miocene to the Pleistocene (Weiss, 1990; Renken, 1998). These three aquifers together are also known as the Southern Hills regional aquifer system (Buono, 1983). Both the Southern Hills regional aquifer system and the Chicot aquifer system are designated as the Sole Source Aquifers (SSA) by the U.S. Environmental Protection Agency.

More than 90% of groundwater use in Louisiana is for agriculture, industry and public supply. 66% of the total groundwater withdrawal are from the Chicot aquifer system and MRAA (Collier and Sargent,

2018). Although groundwater is an abundant source, there are concerns regarding aquifers in Louisiana, such as declined groundwater level due to heavy pumping, contamination from agricultural chemicals, hazardous-waste sites and surface disposals, and saltwater encroachment (Stuart et al., 1994).

3.1. Big well log data

The number of drillers' logs are much greater than the number of geotechnical borings and electric logs. Drillers' logs can provide good lithologic information for shallow depths (e.g., less than 100 m). For the lithofacies modeling drillers' logs, geotechnical borings, and electric logs were interpreted into either sand facies or clay facies. Sand facies represents a group of relatively coarse-grained sediments (e.g., gravel and sand) that have relatively high hydraulic conductivity and form aquifers. Silt, clay, and shale represent a group of relatively fine-grained sediments that have relatively low hydraulic conductivity and form aquitards and aquicludes.

More than 12,000 electric logs and more than 102,000 drillers logs and geotechnical borings (Fig. 5) in Louisiana were collected from the Louisiana Department of Natural Resources, the U.S. Geological Survey (USGS), and the Louisiana Geological Survey. There are more than 355,000 sand and clay facies intervals in the well log data. While the well data distribution is not uniform, on average one well log covers about 1 km^2. Well logs were digitized and interpreted into sand facies and clay facies following the method in Elshall et al. (2013) and Pham and Tsai (2017). Lithologic information in drillers' logs was considered only down to a depth of 107 m (350 feet) while electric logs of water wells can be as deep as 914 m (3000 feet). The number of lithofacies intervals identified in well logs varies from 1 to 76. About 6% of the well logs in Eocene-Pleistocene formations have surficial sand records. 23% of the well logs cover the alluvial formations of the Mississippi River and the Red River.

3.2. Tessellation

Dip directions and dip angles in Louisiana were derived from USGS' regional stratigraphy studies in the south-central United States (Hosman, 1996; Weiss, 1990). Accordingly, this study tessellated Louisiana into 375 tiles shown in Fig. 6. Each tile size is 20 km. The tiles with

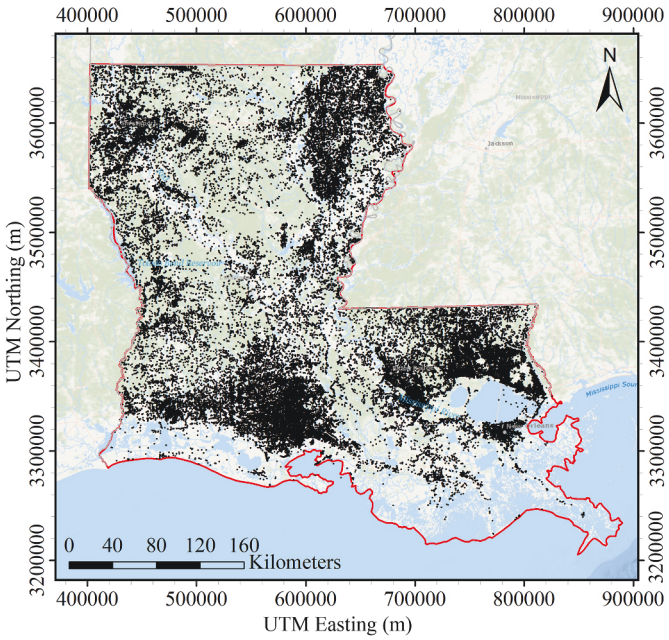

Fig. 5. Location of well logs (black dots) used for lithofacies modeling.

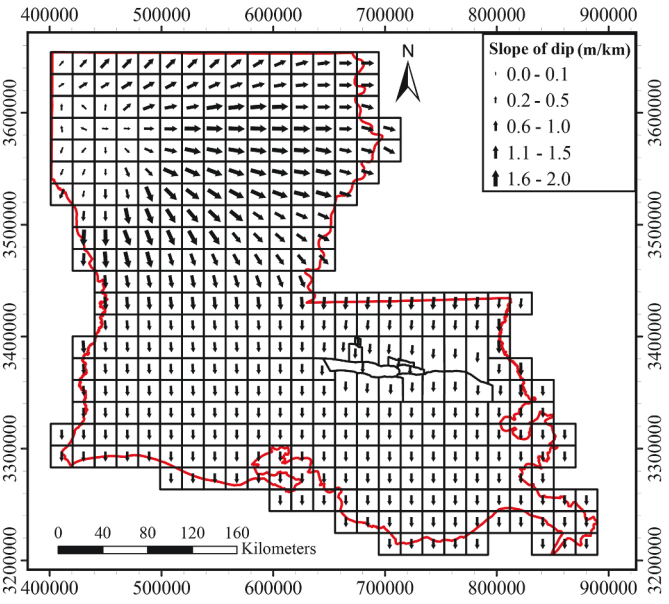

Fig. 6. Tile configuration for the lithofacies model of Louisiana. The vectors show the dip direction for each tile. Thickness of vectors represents the magnitude of the slope. The MRAA and RRAA slope and dip direction are not included.

irregular shape in the southeast were generated to fit fault traces. The tile size is subjective, so is the tile geometry. If needed, the tiles can be refined to account for rapid change in dip direction. Nevertheless, the tessellation in Fig. 6 sufficiently captures the regional dip directions and fault lines. Dip direction and slope in each tile are represented by a vector and its magnitude. In general, formations in the north-central Louisiana dip east toward the axis of the Mississippi embayment (Hosman, 1996). Formations in South Louisiana dip south uniformly, better known as the homocline of the Gulf Coast (Granata, 1963). The truncated Sabine Uplift domal shape indicates that the overlying formations extend outward from the center of the dome and the formation slope increases when moving away from the center (Ewing, 2009). The southern extent of the Sabine Uplift dips south towards the Gulf of Mexico.

It was considered that slopes of dips start from zero at the center of the Sabine Uplift and smoothly increase to 2 m/km (0.002) outward (Ewing, 2009). The slope of Gulf Coast homocline is considered to be 1.5 m/km (0.0015) (Jones et al., 1956). The transition between 1.5 m/km and 2.0 m/km was obtained through vector interpolation. For simplicity, the slope remains the same in depth. The dip direction to the south with a gentle slope of 0.1 m/km (0.0001) is considered for the MRAA and the RRAA. Angular unconformities occur between the alluvial formations and their underneath steeper formations.

3.3. Surface discretization

Each tile was discretized into computational cells of 1 km. However, special refinement around the Baton Rouge fault system was made by nested quadtree grid cells as shown in Fig. 7. Nested quadtree structures were created based on recursive bisectional decomposition of the parent grid (Lien et al., 2015). The cell size gradually decreases from 1 km to 50 m at fault traces. The total number of computational cells at land surface for the Louisiana model is more than 174,000. The vertical resolution for the non-dipping domain is about 3 m (10 feet). The vertical extent is about 900 m, which yields 300 horizontal planes.

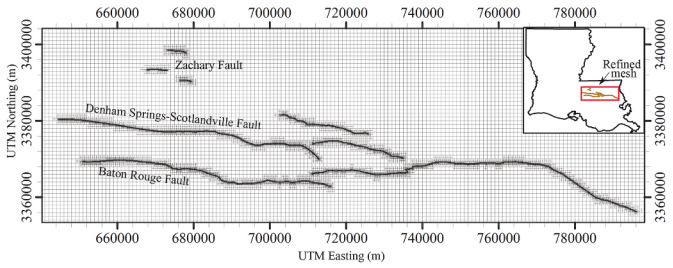

Fig. 7. Computational cells around the Baton Rouge fault system. Base grid resolution is 1 km. Cell size along the fault traces is 50 m.

4. Results and discussions

4.1. Computation time

The lithofacies model for Louisiana was set up and run on a supercomputer at the High Performance Computing (HPC) center at the Louisiana State University. The computation time was around 14 h without parallel computing and was reduced to less than 1 h with the parallel code for computing 375 tiles. The computation time for larger tiles was longer than small tiles.

4.2. Surficial characteristics

Surficial distributions of sand facies and clay facies shown in Fig. 8 suggest 12.4% of land in Louisiana to be potential outcrops of high-permeability facies. The result confirms the outcrop zones of the Southern Hills regional aquifer system in southeastern Louisiana (Buono, 1983), outcrop zones of the Chicot aquifer system and the Evangeline aquifer in west-central Louisiana (Jones et al., 1956), and outcrop zones of the Sparta aquifer in northwestern Louisiana (Ryals, 1982). Fig. 8 also shows potentially limited superficial recharge to the MRAA, which accords with Ackerman (1989), and the RRAA. Southern Louisiana is mostly covered by low-permeability facies. The lithofacies model reveals that the Chenier Plain is mostly fine-grained at surface with a few lenticular sands dispersed across the plain (Byrne et al., 1959; Owen, 2008).

Depth to the topmost sands has tremendous implications on surficial groundwater recharge and groundwater accessibility. The topmost sands in this study are considered to have thickness 6.1 m (20 feet) or greater and are shown in Fig. 9a. The topmost sands for the MRAA and RRAA areas refer to their alluvial sands. By defining a high recharge zone as an area with no surficial confining layer, the Chicot aquifer system has high recharge zones of 283 km^2 in its north. The Southern Hills regional aquifer system has high recharge zones of 268 km^2. The Sparta aquifer has high recharge zones of 200 km^2 in its west. No high recharge zone is recognized for the Cockfield aquifer in the north-central region and for the Carrizo-Wilcox aquifer in the northwestern region.

The effect of well log data density is showing in Fig. 9a and the later figures. The modeling results in the coastal zone have relatively large mosaic pattern due to the low data density. As a result, the estimated lithofacies in the coastal zone have relatively large uncertainty.

Depth to the topmost sands is a useful index to evaluate the accessibility to shallow groundwater. It is evident in Fig. 9a that the Chicot aquifer system, MRAA and RRAA are highly accessible by agricultural

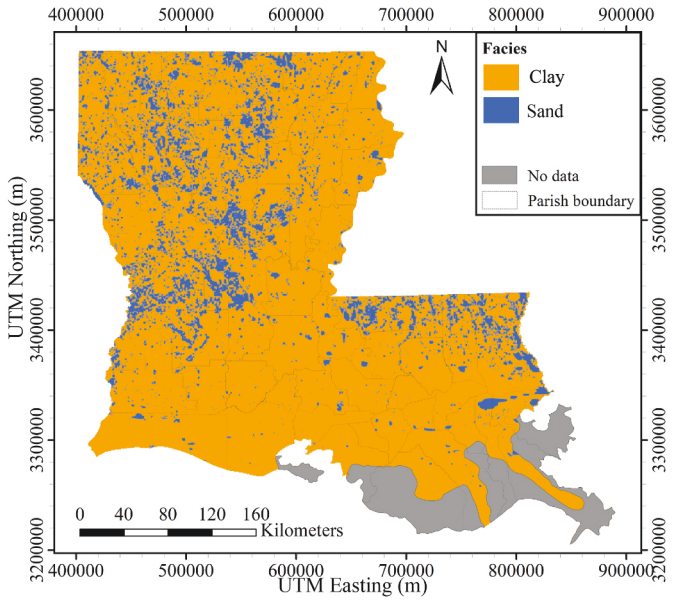

Fig. 8. Distributions of surficial sand facies and surficial clay facies. The gray zones have no well log data in the coastal zone.

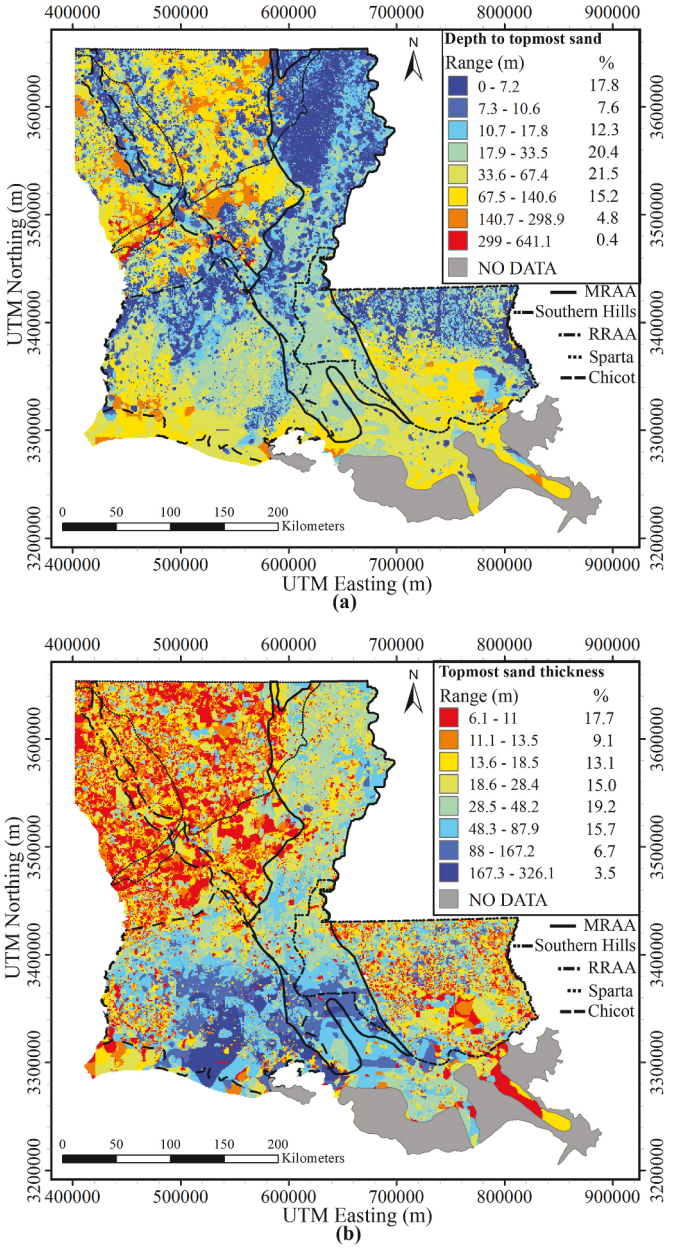

Fig. 9. Maps of topmost sands that have thicknesses greater than 6.1 m (20 ft): (a) depth to topmost sand, and (b) topmost sand thickness.

and industrial wells. The Southern Hills regional aquifer system is also highly accessible by domestic wells in the north of the Baton Rouge Fault. The dense well logs in these regions (Fig. 5) reflect the high aquifer accessibility at relatively shallow depths.

The Chicot aquifer system has much thicker topmost sands than other aquifer systems (Fig. 9b). Topmost sands as thick as 200 m are recognized in the central and eastern areas of the Chicot aquifer where extensive groundwater is extracted for the irrigation purpose. The thickness of the MRAA in the northern area is as high as 60 m and increases towards the south. The northern and central areas of the Southern Hills regional aquifer system have thick topmost sands as well. In contrast, the RRAA and the topmost sands in the Sparta aquifer are thin.

The statistics of top confining units and topmost sands for important aquifers are shown in Table 1. The MRAA has the most uniform top confining unit, whereas the thickness of confining unit of the Sparta aquifer spatially varies the most. Comparing the average values of the depth to the topmost sands, the MRAA and the Sparta aquifer have the best and worst groundwater accessibility, respectively. The range and average of the topmost sand thickness for the Chicot aquifer system indicate that this aquifer has the thickest shallow aquifer sands. On the other hand, the RRAA is thin compared to the other aquifers.

More than 50% of Louisiana is covered with clays thicker than 9.1 m and thinner than 71.1 m (Fig. 10). Thick surficial clays mostly appear in southern Louisiana and in the coastal zone. Fig. 10 is similar to Fig. 9a, where areas with shallow depth to the topmost sands also have thin surficial clay.

4.3. Connections with rivers and lakes

Connections between rivers and lakes and their underlying aquifers were identified. Fig. 11 shows the thickness variation of topmost sands that are connected to the major rivers. The Mississippi River and the Red River are connected to their alluvial sands through around 50% of their river length. Most of the connections along the Mississippi River are identified along its northern extent (Fig. 12). The average sand thickness is higher in the north of the Mississippi River. The decrease in sand thickness from the north to the south of the Mississippi River is probably due to different depositional environments (Saucier, 1994) and reduction in sediment load as the river approaches the Gulf of Mexico (Bentley et al., 2016). In addition, the Atchafalaya River captures around 30% of the Mississippi River flow which causes additional sediment reduction (Roberts, 1997). The Amite River, the Calcasieu River, and the Atchafalaya River are connected to their topmost sands majorly in outcrop zones. The northern reach of the Calcasieu River is connected to the Chicot aquifer system, where the thickness of the topmost sands can be up to 100 m. However, the connection length is very limited to only 14 km. Very limited connection was also found for the Vermilion River. No direct connection was identified between the Mermentau River and its topmost sands as well as the Pearl River and its topmost sands. The Ouachita River and the Sabine River were not analyzed due to the lack of bathymetric data.

Eleven percent (11%) of Lake Catahoula is connected to the MRAA,

Table 1
Statistics of topmost sands for different aquifers or aquifer systems.

Aquifer	Depth to topmost sand (m)			Topmost sand thickness (m)		
	Range	Average	Standard deviation	Range	Average	Standard deviation
Sparta	0–420	70	54	6–140	18	13
Chicot	0–328	36	33	6–326	74	61
Southern Hills	0–424	38	36	6–265	32	27
MRAA	0–91	18	14	6–91	40	19
RRAA	0–91	20	23	6–90	16	8

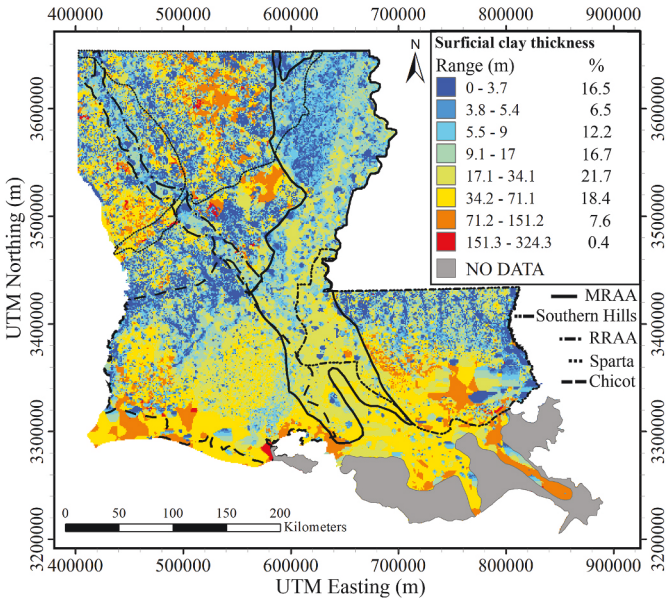

Fig. 10. Map of surficial clay thickness.

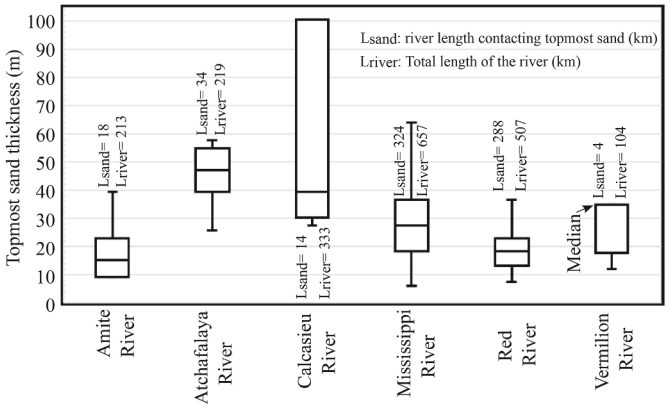

Fig. 11. Thickness of topmost sands contacted by major rivers.

where the thickness of sand is from 28 to 38 m (Fig. 13). The connection area appears in the southwest of the lake (Fig. 12). Lake Pontchartrain is strongly connected to the topmost sands in the southeast. The lake also reaches the Pleistocene sands in the north and Holocene sands in the southwest (Kindinger et al., 1997). No direct connection could be found between other major lakes and their topmost sands. In general, the surface waters in South Louisiana are less likely to be connected to the topmost sands.

4.4. Hydrostratigraphy of western Louisiana

Further analysis is conducted at three north-south cross sections AA', BB', and CC'. The cross section AA' (Fig. 14) illustrates the location of the named aquifers in western Louisiana as well as the domal shape of the Sabine Uplift in the northwest, centered at Bienville Parish. Well logs are relatively shallow in the northwest and deeper in the southwest resulting in greater modeling depths in the southwestern parishes. The names of the hydrogeologic units are referred to Fig. 4b. The cross section AA' shows outcrops of the Upland Terrace sand in the northwest, which is underlain by the Carrizo-Wilcox aquifer formed from deposits of the Wilcox Group and Carrizo Sand Formation (Ryals, 1982). The Carrizo-Wilcox aquifer extends southward to Sabine Parish. The Sparta aquifer outcrops in Webster and Bienville Parishes and is separated from

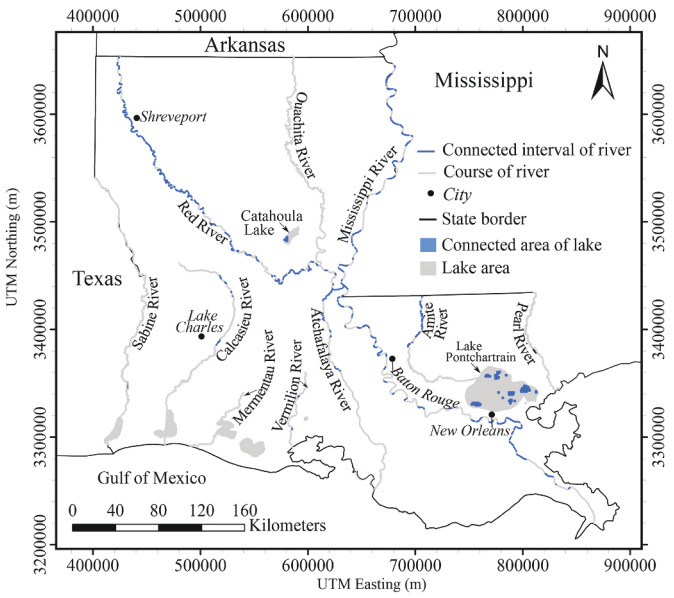

Fig. 12. The connection intervals of the rivers and lakes with their underneath topmost sands.

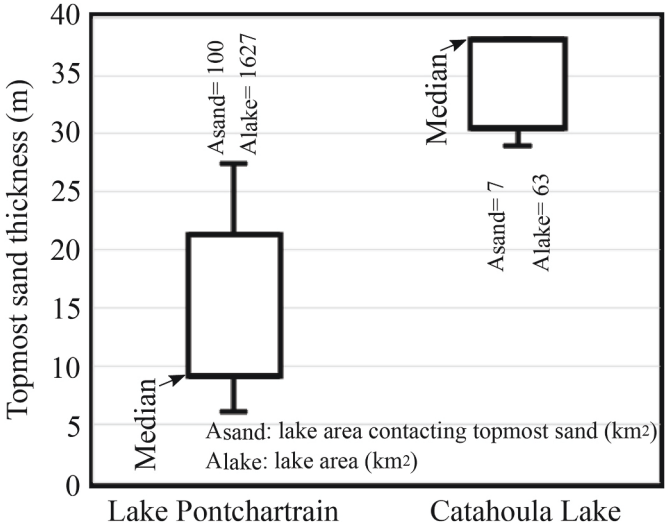

Fig. 13. Thickness of topmost sands contacted by major lakes.

the underlying Carrizo-Wilcox aquifer by the Cane River confining unit (Hosman, 1996). The shallow RRAA is hydraulically connected to the Red River. The Catahoula aquifer outcrops in the southern Sabine Uplift, and is overlain by the Jasper aquifer in Vernon Parish. The Jasper aquifer outcrops in Vernon Parish and is overlain by the Evangeline aquifer in Beauregard parish. The Chicot aquifer system outcrops in Vernon and Beauregard Parishes. The Chicot aquifer system includes three named aquifers (200-foot sand, 500-foot sand and 700-foot sand) in the Lake Charles area (Nyman et al., 1990) and in the western Cameron Parish. The Chicot aquifer system overlies the Evangeline aquifer.

Lithofacies discontinuities shown in Fig. 14 and other cross sections appears in deep depths at some tile boundaries are due to the tessellation effect that creates discontinuous dip direction and dip angle across tile boundaries. The lack of deep wells makes the interpolation discontinuities more pronouncing. Estimated lithofacies at upper depths exhibit less interpolation discontinuities at tile boundaries because of abundant shallow wells. Lithofacies discontinuities occurring within a tile are the result of abrupt lithofacies change in neighboring well logs and the use of the natural neighbor interpolation method. Currently, it is not known whether these are natural lithofacies limits or the results of undiscovered faults.

4.5. Hydrostratigraphy of central Louisiana

Geological characteristics from the north-central Louisiana to the south-central Louisiana are shown in cross section BB' (Fig. 15). The MRAA stretches from Morehouse Parish to St. Landry Parish. The alluvial aquifer is underlain by the Cockfield aquifer in the north-central parishes. The stratigraphy model reveals connections between the MRAA and the Cockfield aquifer in the north (Hosman, 1996). The Cockfield aquifer is separated from the underlying Sparta aquifer by the Cook Mountain confining unit. An angular unconformity is clearly visible in the south-central parishes, where the relatively flat MRAA lies on the top of the relatively steep Chicot aquifer. The Chicot aquifer system includes two named aquifers (Upper Chicot and Lower Chicot) in the east of the aquifer system. The MRAA has an extensive contact (around 1000 km^2) with the Upper Chicot aquifer from St. Landry Parish to Iberia Parish (Weiss, 1990). This contact implies that groundwater exchange between the MRAA and the Upper Chicot aquifer may occur (Nyman et al., 1990). The MRAA is also referred to as the Atchafalaya River alluvial aquifer in this region because of the presence of the Atchafalaya River. The Upper Chicot aquifer can be as thick as 275 m. The average sand thickness in the contact area is 113 m.

4.6. Hydrostratigraphy of Southeast Louisiana

Geological characteristics in southeastern Louisiana exhibit two interesting depositional environments as shown in Fig. 16. The closely interbedded deposit of sand and clay occurs to the north of the Baton Rouge fault, whereas relatively continuous sands occur to the south. Many freshwater aquifers have been named in the St. Helena and Livingston Parishes down to the Catahoula aquifer. The area to the south of the Baton Rouge fault has four named aquifers: the Gramercy aquifer, the Norco aquifer, the Gonzales-New Orleans aquifer, and the 1200-foot sand, all of which are part of the Chicot Equivalent aquifer.

The two different depositional environments may either be related to undiscovered faults in the north creating the disturbed sand beds, or to the source of progradation of Louisiana's coastal plain. There are two substantial hypotheses on the source of progradation (Bentley et al., 2016). Saucier (1994) suggested that the Mississippi River is the only one major fluvial axis, to which all other tributaries join. However, Galloway et al. (2011) suggested the existence of multiple fluvial axes, such as the Mississippi River and the Tennessee River. Saucier's hypothesis would result in a single depositional pattern like the one to the south of the Baton Rouge fault in Fig. 16. However, the multi-axis hypothesis much better complies with the modeling result. The closely interbedded deposit of sand and clay may be further elucidated by the lenticular depositional pattern in the Citronelle Formation (Matson, 1916). Post-depositional faults might have further amplified the close interbedding. The Citronelle Formation is buried by the Pleistocene river terraces where the close interbedding is less conspicuous. More research is necessary to prove that multiple faults in the north of the Denham Springs-Scotlandville fault do exist.

The east-west extents of lithofacies in Louisiana shown in cross sections DD', EE', and FF' are available in the Supplementary Material. The additional cross sections help the understanding of the hydrogeology in Louisiana.

4.7. Major alluvial aquifers

A 3D plot of the sand distribution of the RRAA and the MRAA is shown in Fig. 17. The sand distribution of the RRAA has lenticular characteristics. The vertical extent of the alluvial aquifers is based on the

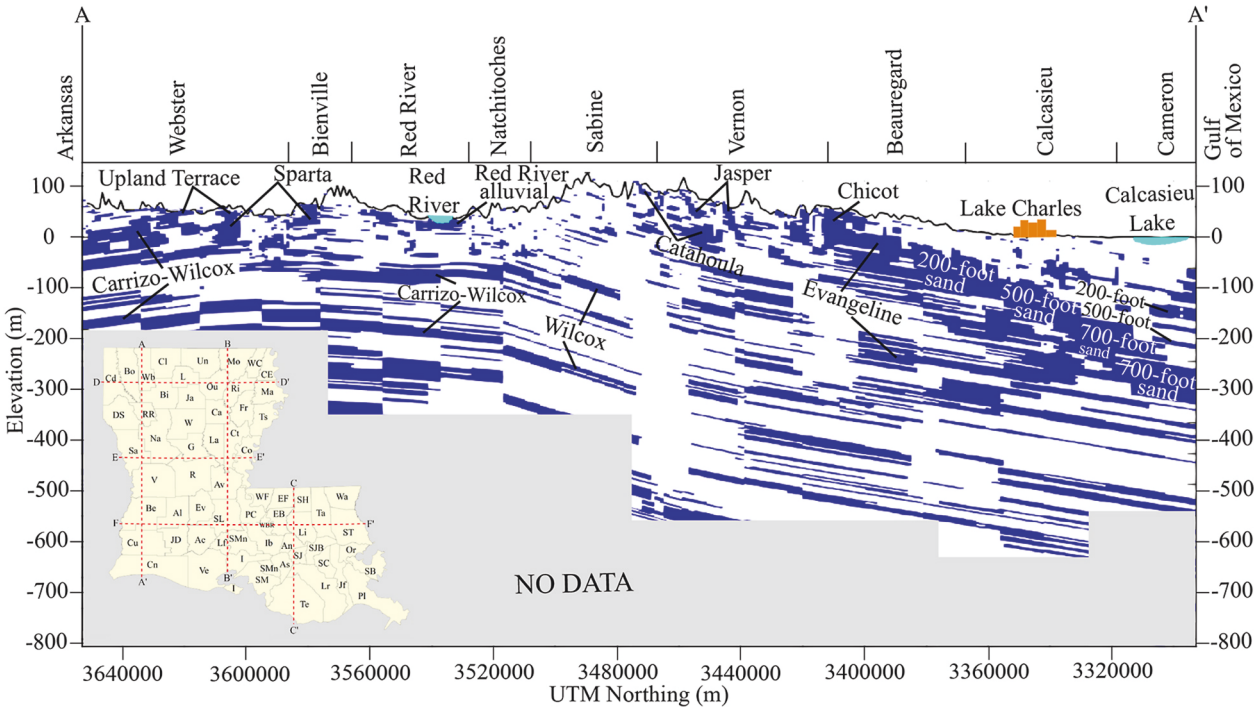

Fig. 14. Sand distributions (blue color) at cross section AA' at UTM zone 15 N Easting 465,000 m. (For interpretation of the references to color in this figure legend, the reader is referred to the Web version of this article.)

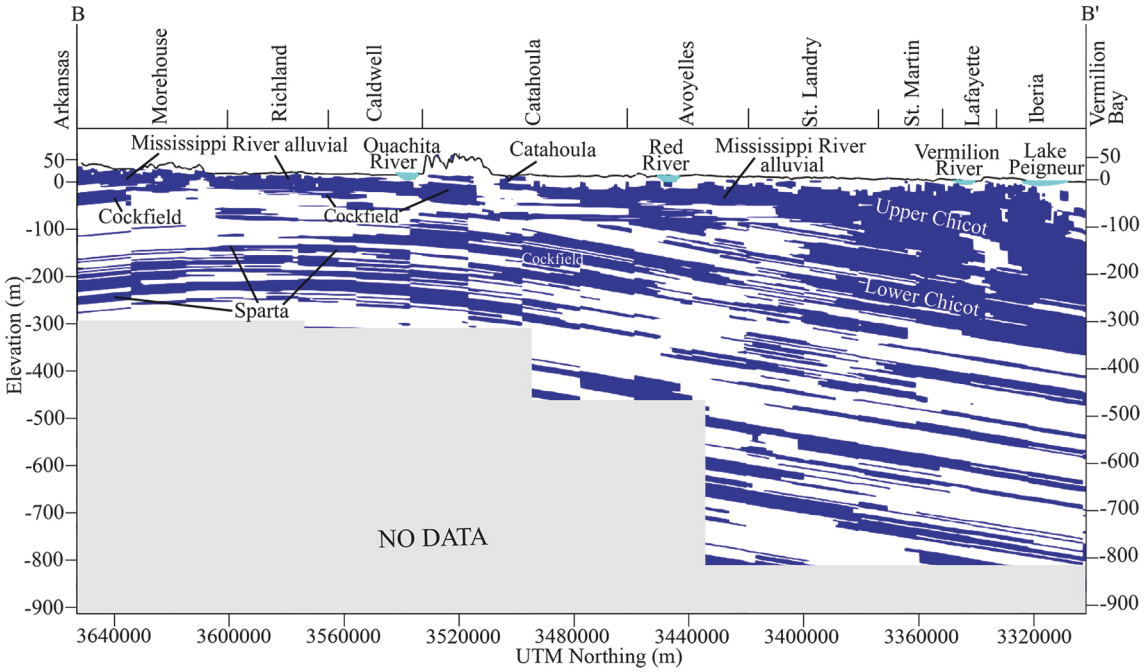

Fig. 15. Sand distributions (blue color) at cross section BB' at UTM zone 15 N Easting 600,000 m. (For interpretation of the references to color in this figure legend, the reader is referred to the Web version of this article.)

USGS Fact Sheets (USGS, 2020). Less than 29% of the Red River alluvial deposits are composed of sand. The lower interconnections are the results of downcutting, erosive actions of the Red River. Sand units in northwestern Louisiana on the other hand are well connected and occur close to land surface (Fig. 9a), indicating potentially strong interactions of the Red River and its alluvial aquifer. The average sand thickness is around 8 m. The total sand volume in the RRAA is approximately 600 million m^3. The RRAA and the MRAA merge in Rapides Parish. 51% of the Mississippi River alluvial deposits are composed of sand. The MRAA is thick and extensive. A relatively thin top confining unit in the north (Fig. 9a) provides favorable conditions for accessing groundwater. The average sand thickness of the MRAA increases from an average of 17 m in the north to an average of 42 m in the south. The total sand volume of the MRAA is around 3900 million m^3.

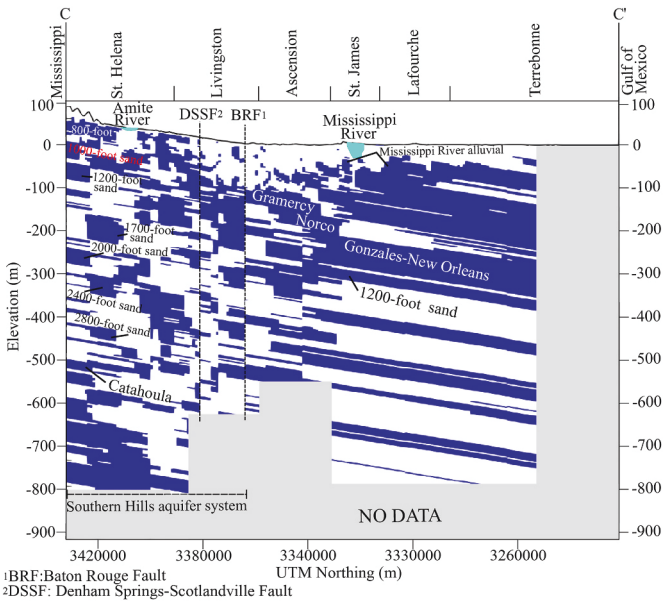

Fig. 16. Sand distributions (blue color) at cross section CC' at UTM zone 15 N Easting 707,000 m. (For interpretation of the references to color in this figure legend, the reader is referred to the Web version of this article.)

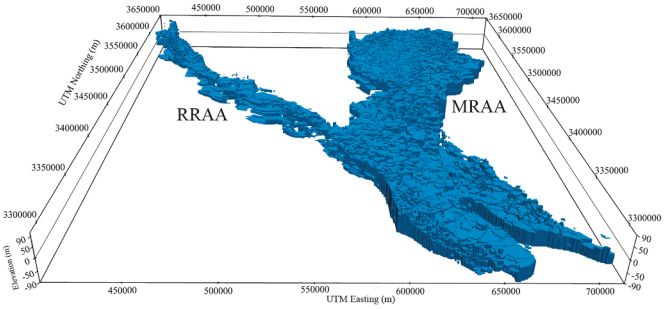

Fig. 17. Sand distributions of the MRAA and the RRAA.

5. Conclusions

The proposed lithofacies modeling method is simple, but efficient to deal with a vast amount of well logs over a very large region. The method accounts for the geologic information (dip direction, dip angle, strike) from the structural geology and transforms the structural information into a non-dipping domain for lithofacies interpolation. The method has been successfully demonstrated to handle distinct geological features in Louisiana (such as angular unconformities, domes, and faults) through domain tessellation, tile discretization, vertical translation, and lithofacies interpolation.

Hydrogeological characteristics were identified for the state of Louisiana through developing a complex lithofacies model. There are three major outcrop zones in northwestern, southeastern, and west-central Louisiana, through which precipitation and surface water recharge the aquifer systems. Southern Louisiana is mostly covered by low-permeability sediments. The average thickness of the top confining layers for the MRAA and the RRAA is around 20 m, which indicates high accessibility to groundwater in these aquifers. The stratigraphy model also reveals that the Mississippi River alluvial aquifer has a strong connection to the sands of both the Upper Chicot and Lower Chicot aquifers.

Assessing the connections between the major rivers and the aquifers reveals that the Mississippi River and the Red River are strongly connected to the MRAA and the RRAA, respectively. The connections between the Mississippi River and its sands mostly occur in the northern reach of the river, whereas the connections become weaker in the Mississippi River Delta. The Calcasieu River, the Atchafalaya River, and the Amite River are all mostly connected to their underlying aquifer systems in the outcrop zones. Catahoula Lake connects to the MRAA. Lake Pontchartrain have connections with shallow sands in many areas.

Sand formations in southeastern Louisiana show two different patterns. The closely interbedded deposit of sand and clay is identified to the north of the Baton Rouge fault while the sand formations to the south of the fault are continuous. The modeled difference between these two patterns of sand formations corresponds well with the hypothesis of multi-axis depositional patterns of the ancestral Mississippi River and Tennessee River. The close interbedding has also been confirmed through the studies on the Citronelle Formation in southeastern Louisiana.

This study does not include uncertainty analysis. The sources of error in the facies modeling results likely come from well log quality, well log interpretation, domain tessellation, tile discretization, interpolation methods, etc. Uncertainty quantification for such a large-scale complex lithofacies model remains a challenging future work.

Declaration of competing interest

The authors declare that they have no known competing financial interests or personal relationships that could have appeared to influence the work reported in this paper.

Acknowledgements

This study was supported in part by the U.S. Geological Survey under Grant/Cooperative Agreement No. G16AP00056, the U.S. National Science Foundation (Award No. 2019561) and the Charles Lamar Family Foundation through Louisiana State University Foundation. Dr. Guillaume Caumon and two anonymous reviewers are acknowledged for their constructive comments. The authors acknowledge the LSU High Performance Computing for providing a supercomputer for this study.

Appendix A. Supplementary data

Supplementary data to this article can be found online at https://doi.org/10.1016/j.cageo.2021.104687.

Data availability

Part of well logs data are available at https://sites.google.com/site/louisianawelllogportal/. Complete well log dataset is available upon request to Frank Tsai.

Computer code availability

Computer code, examples and their results are available in the GitHub, https://github.com/FrankTsai-1/Stratigraphy-Modeling together with instruction.

References

Ackerman, D.J., 1989. Hydrology of the Mississippi River Valley alluvial aquifer, south-central United States; a preliminary assessment of the regional flow system, Water-Resources Investigations Report 88-4028. US Geological Survey 74. https://doi.org/10.3133/wri884028.

ASTM (American Society for Testing and Materials), 2017. Standard Practice for Classification of Soils for Engineering Purposes (Unified Soil Classification System). ASTM International, West Conshohocken, PA, p. D2487. https://doi.org/10.1520/D2487-17.

Bentley Sr, S.J., Blum, M.D., Maloney, J., Pond, L., Paulsell, R., 2016. The Mississippi River source-to-sink system: perspectives on tectonic, climatic, and anthropogenic influences, Miocene to Anthropocene. Earth Sci. Rev. 153, 139–174. https://doi.org/10.1016/j.earscirev.2015.11.001.

Boissonnat, J.D., Cazals, F., 2002. Smooth surface reconstruction via natural neighbour interpolation of distance functions. Comput. Geom. 22 (1–3), 185–203. https://doi.org/10.1016/S0925-7721(01)00048-7.

Buono, A., 1983. The Southern Hills Regional Aquifer System of Southeastern Louisiana and Southwestern Mississippi, Water-Resources Investigations Report 83-4189. US Geological Survey, p. 43. https://doi.org/10.3133/wri834189.

Byrne, J.V., LeRoy, D.O., Riley, C.M., 1959. The Chenier plain and its stratigraphy, southwestern Louisiana. Gulf Coast Association of Geological Societies Transactions 9, 237–260.

Catuneanu, O., Galloway, W.E., Kendall, C.G.S.C., Miall, A.D., Posamentier, H.W., Strasser, A., Tucker, M.E., 2011. Sequence stratigraphy: methodology and nomenclature. Newsl. Stratigr. 44 (3), 173–245. https://doi.org/10.1127/0078-0421/2011/0011.

Catuneanu, O., 2019. Model-independent sequence stratigraphy. Earth Sci. Rev. 188, 312–388. https://doi.org/10.1016/j.earscirev.2018.09.017.

Caumon, G., Collon-Drouaillet, P.L.C.D., De Veslud, C.L.C., Viseur, S., Sausse, J., 2009. Surface-based 3D modeling of geological structures. Math. Geosci. 41 (8), 927–945. https://doi.org/10.1007/s11004-009-9244-2.

Chang, Y.S., Park, H.D., 2004. Development of a web-based geographic information system for the management of borehole and geological data. Comput. Geosci. 30 (8), 887–897. https://doi.org/10.1016/j.cageo.2004.07.006.

Chesnaux, R., Lambert, M., Walter, J., Fillastre, U., Hay, M., Rouleau, A., Daigneault, R., Moisan, A., Germaneau, D., 2011. Building a geodatabase for mapping hydrogeological features and 3D modeling of groundwater systems: application to the Saguenay–Lac-St.-Jean region, Canada. Comput. Geosci. 37 (11), 1870–1882. https://doi.org/10.1016/j.cageo.2011.04.013.

Chilès, J.P., Delfiner, P., 2009. Geostatistics: Modeling Spatial Uncertainty. John Wiley and Sons, p. 734.

Collier, A., Sargent, B.P., 2018. Water Use in Louisiana, 2015. Water Resources Special Report 18. Louisiana Department of Transportation and Development, Baton Rouge, LA, p. 138.

D'Agnese, F.A., Faunt, C.C., Hill, M.C., Turner, A.K., 1999. Death Valley regional groundwater flow model calibration using optimal parameter estimation methods and geoscientific information systems. Adv. Water Resour. 22 (8), 777–790. https://doi.org/10.1016/S0309-1708(98)00053-0.

de Graaf, I.E.M., Sutanudjaja, E.H., van Beek, L.P.H., Bierkens, M.F.P., 2015. A high-resolution global-scale groundwater model. Hydrol. Earth Syst. Sci. 19, 823–837. https://doi.org/10.5194/hess-19-823-2015.

Döll, P., Schmied, H.M., Schuh, C., Portmann, F.T., Eicker, A., 2014. Global-scale assessment of groundwater depletion and related groundwater abstractions: combining hydrological modeling with information from well observations and GRACE satellites. Water Resour. Res. 50 (7), 5698–5720. https://doi.org/10.1002/2014WR015595.

Dowd, P.A., 1991. A review of recent developments in geostatistics. Comput. Geosci. 17 (10), 1481–1500. https://doi.org/10.1016/0098-3004(91)90009-3.

Elshall, A.S., Tsai, F.T.-C., Hanor, J.S., 2013. Indicator geostatistics for reconstructing Baton Rouge aquifer-fault hydrostratigraphy, Louisiana, USA. Hydrogeol. J. 21 (8), 1731–1747. https://doi.org/10.1007/s10040-013-1037-5.

Ewing, T.E., 2009. The ups and downs of the Sabine Uplift and the northern Gulf of Mexico Basin: jurassic basement blocks, Cretaceous thermal uplifts, and Cenozoic flexure. Gulf Coast Association of Geological Societies Transactions 59, 253–269.

Gallerini, G., De Donatis, M., 2009. 3D modeling using geognostic data: the case of the low valley of Foglia river (Italy). Comput. Geosci. 35 (1), 146–164. https://doi.org/10.1016/j.cageo.2007.09.012.

Galloway, W.E., Whiteaker, T.L., Ganey-Curry, P., 2011. History of Cenozoic North American drainage basin evolution, sediment yield, and accumulation in the Gulf of Mexico basin. Geosphere 7 (4), 938–973. https://doi.org/10.1130/GES00647.1.

Goderniaux, P., Brouyère, S., Fowler, H.J., Blenkinsop, S., Therrien, R., Orban, P., Dassargues, A., 2009. Large scale surface–subsurface hydrological model to assess climate change impacts on groundwater reserves. J. Hydrol. 373 (1–2), 122–138. https://doi.org/10.1016/j.jhydrol.2009.04.017.

Granata, W.H., 1963. Cretaceous stratigraphy and structural development of the Sabine Uplift area, Texas and Louisiana. Shreveport Geological Society 5, 84.

Green, P.J., Sibson, R., 1978. Computing Dirichlet tessellations in plane. Comput. J. 21 (2), 168–173. https://doi.org/10.1093/comjnl/21.2.168.

Halbouty, M.T., Halbouty, J.J., 1982. Relationships between east Texas field region and sabine uplift in Texas. Am. Assoc. Petrol. Geol. Bull. 66 (8), 1042–1054.

Haq, B.U., 1991. Sequence stratigraphy, sea-level change, and significance for the deep sea. In: Macdonald, D.I.M. (Ed.), Sedimentation, Tectonics and Eustasy: Sea-Level Changes at Active Margins, vol. 12. Special Publications of The International Association of Sedimentologists, pp. 3–39.

He, X., Koch, J., Sonnenborg, T.O., Jørgensen, F., Schamper, C., Refsgaard, J.C., 2014. Transition probability-based stochastic geological modeling using airborne geophysical data and borehole data. Water Resour. Res. 50 (4), 3147–3169. https://doi.org/10.1002/2013WR014593.

Heinrich, P.V., 2005. Distribution and origin of fault-line scarps of southwest Louisiana, USA, 55. Gulf Coast Association of Geological Societies Transactions, pp. 284–293.

Hilchie, D.W., 1982. Applied Openhole Log Interpretation for Geologists and Engineers (Revised). Douglas W. Hilchie Inc., Golden, Colorado.

Horton, J.D., 2017. The state geologic map compilation (SGMC) geodatabase of the conterminous United States: U.S. Geological survey data release. https://doi.org/10.5066/F7WH2N65.

Hosman, R.L., 1996. Regional stratigraphy and subsurface geology of cenozoic deposits, Gulf coastal plain, south-central United States, professional paper 1416- G. US Geological Survey 48. https://doi.org/10.3133/pp1416G.

Hu, L.Y., Chugunova, T., 2008. Multiple-point geostatistics for modeling subsurface heterogeneity: a comprehensive review. Water Resour. Res. 44 (11) https://doi.org/10.1029/2008WR006993.

Johnson, N.M., 1995. Characterization of alluvial hydrostratigraphy with indicator semivariograms. Water Resour. Res. 31 (12), 3217–3227. https://doi.org/10.1029/95WR02571.

Johnson, N.M., Dreiss, S.J., 1989. Hydrostratigraphic interpretation using indicator geostatistics. Water Resour. Res. 25 (12), 2501–2510. https://doi.org/10.1029/WR025i012p02501.

Jones, P.H., Hendricks, E.L., Irelan, B., 1956. Water Resources of Southwestern Louisiana, Water Supply Paper 1364. US Government Printing Office, p. 460. https://doi.org/10.3133/wsp1364.

Jørgensen, F., Høyer, A.S., Sandersen, P.B., He, X., Foged, N., 2015. Combining 3D geological modelling techniques to address variations in geology, data type and density–An example from Southern Denmark. Comput. Geosci. 81, 53–63. https://doi.org/10.1016/j.cageo.2015.04.010.

Journel, A.G., Alabert, F., 1989. Non-Gaussian data expansion in the earth sciences. Terra. Nova 1 (2), 123–134. https://doi.org/10.1111/j.1365-3121.1989.tb00344.x.

Katal, A., Wazid, M., Goudar, R.H., 2013. Big data: issues, challenges, tools and good practices. In: 2013 Sixth International Conference on Contemporary Computing (IC3). IEEE, pp. 404–409. https://doi.org/10.1109/IC3.2013.6612229.

Kindinger, J.L., Williams, S.J., Penland, S., Flocks, J.G., Connor, P., 1997. Holocene geologic framework of Lake Pontchartrain Basin and lakes of southeastern Louisiana. Gulf Coast Association of Geological Societies 47, 635–638.

Lee, S.Y., Carle, S.F., Fogg, G.E., 2007. Geologic heterogeneity and a comparison of two geostatistical models: sequential Gaussian and transition probability-based geostatistical simulation. Adv. Water Resour. 30 (9), 1914–1932. https://doi.org/10.1016/j.advwatres.2007.03.005.

Lemon, A.M., Jones, N.L., 2003. Building solid models from boreholes and user-defined cross-sections. Comput. Geosci. 29 (5), 547–555. https://doi.org/10.1016/S0098-3004(03)00051-7.

Lien, J.-M., Liu, G., Langevin, C.D., 2015. GRIDGEN version 1.0: a computer program for generating unstructured finite-volume grids. U.S. Geological Survey Open-File Report 2014– 1109, 26. https://doi.org/10.3133/ofr20141109.

Liu, Y., Harding, A., Abriel, W., Strebelle, S., 2004. Multiple-point simulation integrating wells, three-dimensional seismic data, and geology. Am. Assoc. Petrol. Geol. Bull. 88 (7), 905–921. https://doi.org/10.1306/02170403078.

2019 synopsis of current three-dimensional geological mapping and modelling in geological survey organizations; Alberta Energy Regulator/Alberta Geological Survey, AER/AGS Special Report 112. In: MacCormack, K.E., Berg, R.C., Kessler, H., Russell, H.A.J., Thorleifson, L.H. (Eds.), 2019, p. 307. https://ags.aer.ca/publications/SPE_112.html#summary.

Mallet, J.L., 2004. Space–time mathematical framework for sedimentary geology. Math. Geol. 36 (1), 1–32. https://doi.org/10.1023/B:MATG.0000016228.75495.7c.

Mallet, J.L., 2014. Elements of Mathematical Sedimentary Geology: the GeoChron Model. European Association of Geoscientists and Engineers (EAGE) Publications, p. 374.

Matson, G.C., 1916. The pliocene Citronelle Formation of the Gulf coastal plain, professional paper 98- L. US government printing office. https://doi.org/10.3133/pp98L.

Maxwell, R.M., Condon, L.E., Kollet, S.J., 2015. A high-resolution simulation of groundwater and surface water over most of the continental US with the integrated hydrologic model ParFlow v3. Geosci. Model Dev. (GMD) 8, 923–937. https://doi.org/10.5194/gmd-8-923-2015.

McCulloh, R.P., Heinrich, P.V., 2012. Surface faults of the south Louisiana growth-fault province. GSA (Geol. Soc. Am.) Spec. Pap. (Reg. Stud.) 493, 37–49. https://doi.org/10.1130/2012.2493(03.

Nyman, D.J., Halford, K.J., Martin Jr., A., 1990. Geohydrology and Simulation of Flow in the Chicot Aquifer System of Southwest Louisiana, Water Resources Technical Report 50. Louisiana Department of Transportation and Development, p. 65.

Owen, D.E., 2008. Geology of the Chenier Plain of Cameron parish, southwestern Louisiana. In: Moore, G. (Ed.), Geological Society of America Field Guide 14 2008 Joint Annual Meeting. The Geological Society of America, Houston, Texas. https://doi.org/10.1130/2008.fld014(02, 5–9 October 2008.

Pham, H.V., Tsai, F.T.-C., 2017. Modeling complex aquifer systems: a case study in Baton Rouge, Louisiana (USA). Hydrogeol. J. 25, 601–615. https://doi.org/10.1007/s10040-016-1532-6.

Posamentier, H.W., Allen, G.P., 1993. Siliciclastic sequence stratigraphic patterns in foreland, ramp-type basins. Geology 21 (5), 455–458. https://doi.org/10.1130/0091-7613(1993)021%3C0455:SSSPIF%3E2.3.CO;2.

Posamentier, H.W., James, D.P., 1993. An overview of sequence-stratigraphic concepts: uses and abuses. In: Posamentier, H.W., Summerhayes, C.P., Haq, B.U., Allen, G.P. (Eds.), Sequence Stratigraphy and Facies Associations, vol. 18. Special Publications of The International Association of Sedimentologists, pp. 3–18.

Renken, R.A., 1998. Ground Water Atlas of the United States: Segment 5, Arkansas, Louisiana, Mississippi, Hydrologic Atlas 730- F. US Geological Survey, p. 28. https://doi.org/10.3133/ha730F.

Roberts, H.H., 1997. Dynamic changes of the Holocene Mississippi River delta plain: the delta cycle. J. Coast Res. 13 (3), 605–627.

Royse, K.R., 2010. Combining numerical and cognitive 3D modelling approaches in order to determine the structure of the Chalk in the London Basin. Comput. Geosci. 36 (4), 500–511. https://doi.org/10.1016/j.cageo.2009.10.001.

Ryals, G.N., 1982. Regional geohydrology of the northern Louisiana salt-dome basin: Part I, conceptual model and data needs, open-file report 82-343. US Geological Survey 27. https://doi.org/10.3133/ofr82343.

Saucier, R.T., 1994. Geomorphology and Quaternary Geologic History of the Lower Mississippi Valley. Y: Vicksburg, Mississippi, Waterways Experiment Station. U.S. Army Corps of Engineers, p. 417.

Sivarajah, U., Kamal, M.M., Irani, Z., Weerakkody, V., 2017. Critical analysis of Big Data challenges and analytical methods. J. Bus. Res. 70, 263–286. https://doi.org/10.1016/j.jbusres.2016.08.001.

Smoot, C.W., 1986. Louisiana hydrologic atlas map no. 2: areal extent of freshwater in major aquifers of Louisiana: U.S. Geological Survey Water-Resources Investigations Report 86-4150, 1 Sheet. https://doi.org/10.3133/wri864150.

Song, S., Hou, J., Dou, L., Song, Z., Sun, S., 2020. Geologist-level wireline log shape identification with recurrent neural networks. Comput. Geosci. 134, 104313. https://doi.org/10.1016/j.cageo.2019.104313.

Spiegel, M.R., 1986. Mathematical Handbook of Formulas and Tables., Schaum's Outline Series. McGraw-Hill Publishing Company, New York, p. 271pp.

Strebelle, S., 2002. Conditional simulation of complex geological structures using multiple-point statistics. Math. Geol. 34 (1), 1–21. https://doi.org/10.1023/A:1014009426274.

Stuart, C.G., Knochenmus, D.D., McGee, B.D., 1994. Guide to Louisiana's Ground-Water Resources (Vol. 94, No. 4085). U.S. Geological Survey, Water-Resources Investigations Report 94-4085. USGS Earth Science Information Center, Open-File Reports Section, p. 55. https://doi.org/10.3133/wri944085.

Sukumar, N., Moran, B., Yu Semenov, A., Belikov, V.V., 2001. Natural neighbour Galerkin methods. Int. J. Numer. Methods Eng. 50 (1), 1–27. https://doi.org/10.1002/1097-0207(20010110)50:1%3C1::AID-NME14%3E3.0.CO;2-P.

Sutanudjaja, E.H., van Beek, L.P.H., de Jong, S.M., van Geer, F.C., Bierkens, M.F.P., 2011. Large-scale groundwater modeling using global datasets: a test case for the Rhine-Meuse basin. Hydrol. Earth Syst. Sci. 15, 2913–2935. https://doi.org/10.5194/hess-15-2913-2011.

Touch, S., Likitlersuang, S., Pipatpongsa, T., 2014. 3D geological modelling and geotechnical characteristics of Phnom Penh subsoils in Cambodia. Eng. Geol. 178, 58–69. https://doi.org/10.1016/j.enggeo.2014.06.010.

Tsai, F.T.-C., 2009. Indicator generalized parameterization for interpolation point selection in groundwater inverse modeling. J. Hydrol. Eng. 14 (3), 233–242. https://doi.org/10.1061/(ASCE)1084-0699(2009)14:3(233).

U.S. Census Bureau, 2010. State area measurements and internal point coordinates. https://www.census.gov/geographies/reference-files/2010/geo/state-area.html.

USGS, 2020. U.S. Geological survey, water resources of Louisiana's parishes. https://www.usgs.gov/centers/lmg-water/science/water-resources-louisiana-s-parishes?qt-science_center_objects=0#qt-science_center_objects.

Wackernagel, H., 2013. Multivariate Geostatistics: an Introduction with Applications. Springer Science and Business Media, p. 292pp.

Watson, D., 1999. The natural neighbor series manuals and source codes. Comput. Geosci. 25 (4), 463–466. https://doi.org/10.1016/S0098-3004(98)00150-2.

Weiss, J.S., 1990. Geohydrologic Units of the Coastal Lowlands Aquifer System, South-Central United States, Open-File Report 90-173. Department of the Interior, U.S. Geological Survey; Books and Open-File Reports Section, p. 34. https://doi.org/10.3133/ofr90173.

Weissmann, G.S., Carle, S.F., Fogg, G.E., 1999. Three-dimensional hydrofacies modeling based on soil surveys and transition probability geostatistics. Water Resour. Res. 35 (6), 1761–1770. https://doi.org/10.1029/1999WR900048.

Wu, Q., Xu, H., Zou, X., 2005. An effective method for 3D geological modeling with multi-source data integration. Comput. Geosci. 31 (1), 35–43. https://doi.org/10.1016/j.cageo.2004.09.005.

Wycisk, P., Hubert, T., Gossel, W., Neumann, C., 2009. High-resolution 3D spatial modelling of complex geological structures for an environmental risk assessment of abundant mining and industrial megasites. Comput. Geosci. 35 (1), 165–182. https://doi.org/10.1016/j.cageo.2007.09.001.

Yoshida, S., Steel, R.J., Dalrymple, R.W., 2007. Changes in depositional processes—an ingredient in a new generation of sequence-stratigraphic models. J. Sediment. Res. 77 (6), 447–460. https://doi.org/10.2110/jsr.2007.048.

Zhu, L., Zhang, C., Li, M., Pan, X., Sun, J., 2012. Building 3D solid models of sedimentary stratigraphic systems from borehole data: an automatic method and case studies. Eng. Geol. 127, 1–13. https://doi.org/10.1016/j.enggeo.2011.12.001.